Atherosclerosis 322 (2021) 1–7

Contents lists available at ScienceDirect

Atherosclerosis

journal homepage: www.elsevier.com/locate/atherosclerosis

The feasibility and limitation of coronary computed tomographic angiography imaging to identify coronary lipid-rich atheroma *in vivo*: Findings from near-infrared spectroscopy analysis

Satoshi Kitahara [a,b], Yu Kataoka [a,*], Hiroyuki Miura [a], Tatsuya Nishii [c], Kunihiro Nishimura [d], Kota Murai [a,b], Takamasa Iwai [a], Hayato Nakamura [e], Hayato Hosoda [f], Hideo Matama [a,b], Takahito Doi [a], Takahiro Nakashima [g], Satoshi Honda [a], Masashi Fujino [a], Kazuhiro Nakao [a], Shuichi Yoneda [a], Kensaku Nishihira [h], Tomoaki Kanaya [i], Fumiyuki Otsuka [a], Yasuhide Asaumi [a], Kenichi Tsujita [j], Teruo Noguchi [a,b], Satoshi Yasuda [a,k]

[a] *Department of Cardiovascular Medicine, National Cerebral & Cardiovascular Center, Osaka, Japan*
[b] *Department of Advanced Cardiovascular Medicine, Graduate School of Medical Sciences, Kumamoto University, Kumamoto, Japan*
[c] *Department of Radiology, National Cerebral & Cardiovascular Center, Osaka, Japan*
[d] *Department of Preventive Medicine and Epidemiology, National Cerebral & Cardiovascular Center, Osaka, Japan*
[e] *Division of Internal Medicine, Okinawa Prefectural Yaeyama Hospotal, Ishigaki, Okinawa, Japan*
[f] *Department of Cardiology, Chikamori Hospital, Kochi, Japan*
[g] *Department of Emergency Medicine, University of Michigan, Ann Arbor, MI, USA*
[h] *Department of Cardiology, Miyazaki Medical Association Hospital, Miyazaki, Japan*
[i] *Department of Cardiovascular Medicine, Dokkyo Medical University Hospital, Mibu, Tochigi, Japan*
[j] *Department of Cardiovascular Medicine Graduate School of Medical Sciences, Kumamoto University, Kumamoto, Japan*
[k] *Department of Cardiovascular Medicine, Tohoku University Graduate School of Medicine, Sendai, Miyagi, Japan*

A R T I C L E I N F O

Keywords:
Coronary
Computed tomography
Near-infrared spectroscopy
Lipid-rich plaque

A B S T R A C T

Background: Coronary computed tomography angiography (CCTA) non-invasively visualizes lipid-rich plaque. However, this ability is not fully validated *in vivo*. The current study aimed to elucidate the association of CCTA features with near-infrared spectroscopy-derived lipidic plaque measure in patients with coronary artery disease.
Methods: 95 coronary lesions (culprit/non-culprit = 51/44) in 35 CAD subjects were evaluated by CCTA and NIRS imaging. CT density, positive remodeling, spotty calcification, napkin-ring sign and NIRS-derived maximum 4-mm lipid-core burden index ($maxLCBI_{4mm}$) were analyzed by two independent physicians. The association of CCTA-derived plaque features with $maxLCBI_{4mm} \geq 400$ was evaluated.
Results: The median CT density and $maxLCBI_{4mm}$ were 57.7 Hounsfield units (HU) and 304, respectively. CT density ($r = -0.75$, $p < 0.001$) and remodeling index (RI) ($r = 0.58$, $p < 0.001$) were significantly associated with $maxLCBI_{4mm}$, respectively. Although napkin-ring sign ($p < 0.001$) showed higher prevalence of $maxLCBI_{4mm} \geq 400$ than those without it, spotty calcification did not ($p = 0.13$). On multivariable analysis, CT density [odds ratio (OR) = 0.95, 95% confidence interval (CI) = 0.93–0.97; $p < 0.001$] and positive remodeling [OR = 7.71, 95%CI = 1.37–43.41, $p = 0.02$] independently predicted $maxLCBI_{4mm} \geq 400$. Receiver operating characteristic curve analysis demonstrated CT density <32.9 HU (AUC = 0.92, sensitivity = 85.7%, specificity = 91.7%) and RI ≥ 1.08 (AUC = 0.83, sensitivity = 74.3%, specificity = 85.0%) as optimal cut-off values of $maxLCBI_{4mm} \geq 400$. Of note, only 52.6% at lesions with one of these plaque features exhibited $maxLCBI_{4mm} \geq 400$, whereas the frequency of $maxLCBI_{4mm} \geq 400$ was highest at those with both features (88.5%, $p < 0.001$ for trend).
Conclusions: CT density <32.9 HU and RI ≥ 1.08 were associated with lipid-rich plaque on NIRS imaging. Our findings underscore the synergistic value of CT density and positive remodeling to detect lipid-rich plaque by CCTA.

* Corresponding author. Department of Cardiovascular Medicine, National Cerebral & Cardiovascular Centre, Osaka, Japan, 6-1 Kishibe-shimmachi, Suita, Osaka, 564-8565, Japan
E-mail address: yu.kataoka@ncvc.go.jp (Y. Kataoka).

https://doi.org/10.1016/j.atherosclerosis.2021.02.019
Received 22 October 2020; Received in revised form 4 February 2021; Accepted 18 February 2021
Available online 24 February 2021

1. Introduction

Lipid-rich plaque has been considered as an important substrate of coronary atherosclerosis causing future coronary events [1,2]. Coronary computed tomography angiography (CCTA) non-invasively visualizes lipid-rich plaque based on its computed tomography (CT) density in addition to the presence of positive remodeling, spotty calcification and/or napkin-ring sign [3–6]. Some of these features have been shown to associate with cardiac outcomes [7,8]. However, cut-off value of CT density associated with lipid-rich plaque is inconsistent between clinical observational studies and *ex vivo* validation ones [9–12]. In addition, *in vivo* validation study has not been fully conducted to compare CCTA images with intravascular imaging modality which has sophisticated ability for detecting lipidic plaque burden.

Near-infrared spectroscopy (NIRS) imaging enables to quantitatively evaluate lipid-rich atheroma *in vivo* [13]. It has been shown that maximum 4-mm lipid-core burden index ($maxLCBI_{4mm}$) $\geq$400 corresponds to lipid-rich plaque causing acute coronary syndrome [14]. Given that this measure has been already validated by pathohistological specimen of coronary artery [15,16], this modality provides an opportunity to investigate whether CCTA-derived plaque features accurately identify lipid-rich plaque *in vivo*. Therefore, the current study sought to elucidate the association of CCTA features with NIRS-derived lipidic plaque measure in patients with coronary artery disease (CAD).

2. Patients and methods

2.1. Study population

We retrospectively analyzed 95 consecutive patients with CAD who underwent both clinically indicated CCTA and NIRS/intravascular ultrasound (IVUS) imaging prior to percutaneous coronary intervention (PCI) from August 1, 2015 to November 30, 2020 at the National Cerebral & Cardiovascular Center, Osaka, Japan (Supplementary Fig. 1). Of these, the following subjects were excluded; those imaged by inadequate CCTA imaging protocol (n = 13), patients with poor quality of NIRS/IVUS images (n = 1), a case with in-stent restenosis lesion (n = 1), (n = 1), the interval between CCTA and NIRS/IVUS imaging > 3 months (n = 23) and commencement or dose escalation of any lipid-lowering agents between CCTA and NIRS/IVUS imaging (n = 22). As a consequence, the remaining 35 patients with 95 *de novo* coronary lesions were included into the current study analysis. Written informed consent was not obtained by each subject due to the observational analysis of hospitalized patients. However, the current study was posted on the website of our institution (http://www.ncvc.go.jp/hospital/pub/clinical-research/untersuchung/untersuchung-78.html) to inform about its detail and ensure that patients could refuse inclusion in the current analysis. When we contacted participants by mail or telephone, we explained the study and then obtained informed consent. The study protocol conforms to the ethical guidelines of the 1975 Declaration of Helsinki, and it was approved by the institutional ethics committee (research project number: M30-084-02).

2.2. The definition of analyzed lesions

The current study analyzed both culprit and non-culprit lesions. Culprit lesion was defined as the segment receiving PCI. Non-culprit lesion was defined as (1) a percent diameter stenosis >20% on quantitative coronary angiography and (2) the segment without any history of PCI. If multiple lesions existed in the same vessel, we analyzed individual plaques separated by at least 5-mm from each other.

2.3. CCTA imaging, and its quantitative and qualitative analyses

CCTA was performed using the second and third-generation dual-source CT (DSCT) scanners (SOMATOM Definition Flash and SOMATOM Force; Siemens Healthcare, Forchheim, Germany). Retrospective ECG-gated spiral scan with tube current modulation or prospective ECG triggered high-pitch spiral scan was selected depending on the heart rate. Further scan parameters in the second and third-generation DSCT were as follows: section collimation 2 × 64 × 0.6-mm and 2 × 96 × 0.6-mm, gantry rotation 0.275 s and 0.25 s, respectively. Automated tube current modulation (CARE Dose4D, Siemens) and automatic tube-voltage selection (CARE kV, Siemens) were used with 240–280 mAs as qualified reference tube-current time products and 120-kV as reference tube-voltage. The images were reconstructed using iterative reconstruction (SAFIRE or ADMIRE, Siemens) with 0.6-mm slice thickness and 0.3-mm increments with a medium convolution kernel (I31f or Bv40). The current CCTA imaging protocol complied with the SCCT guidelines for performance of coronary computed tomographic angiography [17].

Plaque CT density (HU=Hounsfield units) at analyzed lesions was quantitatively measured as follows. Firstly, a total of three region of interests (approximately 0.5–1.0 mm^2) were placed at the site exhibiting low CT attenuation within the analyzed lesions throughout visual screening of images. Secondly, CT density at each region of interest was measured and then averaged. Qualitative analysis was performed to evaluate (1) remodeling index (RI), (2) spotty calcification, (3) napkin-ring sign, and (4) low attenuation plaque volume. RI was assessed in multi-planar reformatted images reconstructed in long axis and short axis view of the vessel by the following formula:

RI = (cross-sectional lesion diameter) / (diameter of a proximal reference segment)

Positive remodeling was defined as RI $\geq$ 1.1 [18,19]. Spotty calcification was defined as <3 mm on focal multiplanar reconstruction images and cross-sectional images. Napkin-ring sign was defined as a ring-like peripheral higher attenuation of the non-calcified portion of the coronary plaque. With regard to low attenuation plaque volume, low attenuation was defined as CT value < 32.9 according to our current receiver operating curve analysis. Then, low attenuation area was automatically traced at each cross-sectional image of the analyzed plaques. Low attenuation plaque volume was calculated as the sum of its areas across all cross-sectional images of plaques. These quantitative and qualitative analyses were performed with a software that facilitates plaque volume measurement (Ziostation2, Ziosoft, Tokyo, Japan). CCTA analyses were conducted by two independent researchers, blind to clinical characteristics (SK and HM).

2.4. NIRS imaging

The entire target vessel requiring PCI was evaluated by NIRS/IVUS imaging as reported previously. In detail, after intracoronary administration of nitroglycerin (100-300 μg), the imaging catheter (TVC Insight™ or Dualpro™, Infraredx, Bedford, MA, USA) was automatically pulled back from the most distal site of the target artery at a speed of 0.5 mm/s and 960 rpm (TVC Insight™) or 2.0 mm/s and 1800 rpm (Dualpro™) [20]. Makoto® system (Infraredx, Bedford, MA, USA) was used to analyze the obtained chemogram data [15]. PCI was conducted after the completion of the NIRS/IVUS imaging. $MaxLCBI_{4mm}$ at culprit and non-culprit lesions was used for the analysis [21]. NIRS images were analyzed by physicians who were blind to the clinical characteristics of the patients (SK, KM and YK).

2.5. Quantitative coronary angiography analysis

Quantitative coronary angiography (QCA) analysis was performed at culprit and non-culprit lesions using an off-line commercially available software (QAngio® XA, Medis, Leiden, the Netherlands). QCA analysis included minimal lumen diameter, percent diameter stenosis, lesion length and reference vessel diameter.

2.6. Statistical analysis

Continuous variables were expressed as the mean ± standard deviation and compared using the *t*-test if data were normally distributed. Non-normally distributed continuous data were summarized as the median (interquartile range) and compared using the Wilcoxon rank sum test. Categorical variables were compared using the Fisher exact test or the Chi-square test as appropriate. Spearman's rank-order correlation was used to examine the relationship of $maxLCBI_{4mm}$ with CT density and RI. Linear regression analysis was conducted to determine CCTA plaque featured associated with $maxLCBI_{4mm} \geq 400$. Significant parameters in univariable analysis were entered into the multivariable one. Receiver-operating characteristic curve analyses, and calculations of sensitivity and specificity were performed to analyze the predictive ability of CT density for $maxLCBI_{4mm} \geq 400$. The best cut-off value of CT density was determined by selecting the value which maximized the sum of sensitivity and specificity. According to the study analyzing lipid (n = 40) and non-lipid (n = 15) plaques [22], the expected difference in the frequency of low attenuation plaque is considered as 10% between these two types of plaques. A sample of 59 lesions will be required for 90% power at a two-sided alpha level of 0.05 to detect a nominal difference of 10%, assuming a standard deviation of 10%. All *p*-values <0.05 were considered statistically significant. All analyses were performed with JMP version 14 (SAS Institute, Cary, NC).

3. Results

3.1. Clinical demographics of study subjects

Clinical demographics of the study population are summarized in Table 1. Patients had a mean age of 65 years, 79% were male, and they had a high prevalence of risk factors (hypertension: 74%, dyslipidemia: 86%, type 2 diabetes mellitus: 34%). 77% of the study subjects presented stable CAD. With regard to the use of anti-atherosclerotic medical therapies, statin was already commenced prior to CCTA imaging in most of the study population (30/35 = 86%). Their on-treatment low density lipoprotein cholesterol was 2.20 [1.91–2.72] mmol/l.

3.2. Coronary angiographic features of analyzed lesions

Table 1 shows the angiographic characteristics of the analyzed lesions. The current study analyzed 95 coronary lesions, which included 51 culprit and 44 non-culprit lesions. About 67% of analyzed lesions were located within the left anterior descending artery. There were no significant differences in the location and the frequency of proximal segment of major coronary arteries between culprit and non-culprit lesions (Supplementary Table 1). As expected, culprit lesions were more likely to exhibit a greater % diameter stenosis and a longer lesion length compared to non-culprit ones (Supplementary Table 1).

3.3. CCTA and NIRS measures

On CCTA analysis, the median CT value at analyzed lesions was 57.7 [19.8–103.0] HU and the median RI was 1.00 [0.90–1.17]. Positive remodeling, spotty calcification and napkin-ring sign were observed in 35, 31, and 26% of analyzed lesions, respectively (Table 1). NIRS measures at the corresponding lesions are shown in Table 1. The median $maxLCBI_{4mm}$ was 304 [102-516], and the prevalence of $maxLCBI_{4mm} \geq 400$ was 37%. Supplementary Table 2 presents the comparison of CCTA and NIRS imaging between culprit and non-culprit lesions. Predictably, culprit lesions were more likely to exhibit lower CT value and higher RI and $maxLCBI_{4mm}$ with a greater frequency of positive remodeling and napkin-ring sign (Supplementary Table 2).

Table 1
Baseline clinical characteristics and angiographic, CCTA and NIRS measures.

Baseline clinical characteristics (n = 35 patients)	
Age, years	65 ± 12
Male, n (%)	30 (79%)
Body mass index (kg/m^2)	23.9 (21.9–27.2)
Clinical presentation	
Stable CAD, n (%)	27 (77%)
ACS, n (%)	8 (23%)
Coronary risk factor	
Hypertension, n (%)	26 (74%)
Dyslipidemia, n (%)	30 (86%)
Type 2 diabetes mellitus, n (%)	12 (34%)
Current Smoking, n (%)	7 (20%)
Medication use	
Aspirin, n (%)	29 (83%)
P2Y12 inhibitor, n (%)	31 (89%)
Statin, n (%)	30 (86%)
Ezetimibe, n (%)	7 (20%)
β-blocker, n (%)	22 (63%)
ACE-I/ARB, n (%)	18 (51%)
Laboratory data	
eGFR (mL/min/1.73m^2)	67.3 ± 14.9
LDL-cholesterol (mmol/l)	2.20 (1.91–2.72)
HDL-cholesterol (mmol/l)	1.19 (1.06–1.40)
Triglyceride (mmol/l)	1.46 (0.96–2.27)
Hemoglobin A1c (%)	5.9 (5.5–6.5)
Angiographic findings, CCTA and NIRS measures (n = 95 lesions)	
Culprit lesion, n (%)	51 (53%)
Non-culprit lesion, n (%)	44 (47%)
Location of lesions	
LAD, n (%)	64 (67%)
LCX, n (%)	10 (11%)
RCA, n (%)	21 (22%)
Proximal lesion, n (%)	43 (45%)
QCA analysis	
% diameter stenosis (%)	51.4 (31.0–71.0)
Reference diameter (mm)	3.5 ± 0.7
Lesion length (mm)	18.0 (12.3–26.5)
CCTA findings	
CT density (HU)	57.7 (19.8–103.0)
Remodeling index	1.00 (0.90–1.17)
Positive remodeling (%)	33 (35%)
Spotty calcification (%)	29 (31%)
Napkin-ring sign (%)	25 (26%)
NIRS/IVUS findings	
$MaxLCBI_{4mm}$	304 (102–516)
$MaxLCBI_{4mm} \geq 400$	35 (37%)

ACE-I = angiotensin converting enzyme inhibitor, ACS = acute coronary syndrome, ARB = angiotensin ll receptor blocker, CAD = coronary artery disease, CCTA = coronary computed tomography angiography, CT = computed tomography, eGFR = estimated glomerular filtration rate, HDL = high density lipoprotein, HU = Hounsfield units, LAD = left anterior descending artery, LDL = low density lipoprotein, LCBI = lipid core burden index, LCX = left circumflex artery, $MaxLCBI_{4mm}$ = maximum 4 mm Lipid Core Burden Index, NIRS = near-infrared spectroscopy, RCA = right coronary artery, QCA = quantitative coronary angiography.
Continuous data are presented as means ± standard deviation, if data were normally distributed.
Non-normally distributed continuous data were summarized as the median (interquartile range).

3.4. Relationships between $maxLCBI_{4mm}$ and CCTA measures

Supplementary Figure 2 illustrates the relationship of $maxLCBI_{4mm}$ with CT density and RI. CT density was negatively associated with $maxLCBI_{4mm}$ (r = -0.75, $p < 0.001$, Supplementary Fig. 2A), whereas RI was positively correlated to $maxLCBI_{4mm}$ (r = 0.58, $p < 0.001$, Supplementary Fig. 2B). Additionally, as expected, lesions exhibiting $maxLCBI_{4mm} \geq 400$ were more likely to present a lower CT density [10.3 [-2.0-29.2] HU *vs.* 85.3 [53.6–116.9] HU, $p < 0.001$) and a larger RI [1.18 [1.05–1.35] *vs.* 0.95 [0.88–1.04], $p < 0.001$), accompanied by a greater frequency of napkin-ring sign (51.4% *vs.* 11.7%, $p < 0.001$), whereas the

prevalence of spotty calcification was comparable between two groups (40.0% *vs.* 25.0%, $p = 0.13$) (Fig. 1, A-D).

Uni- and multivariable analyses were conducted to identify an independent CCTA-derived feature associated with maxLCBI$_{4mm} \geq 400$. Univariable analysis demonstrated that CT density, positive remodeling and napkin-ring sign predicted maxLCBI$_{4mm} \geq 400$ at coronary lesions (Table 2). On multivariable analysis, CT density and positive remodeling emerged as the independent predictor of maxLCBI$_{4mm} \geq 400$ (Table 2). Receiver operating characteristic curve analysis determined CT density <32.9 HU (AUC = 0.92, sensitivity = 85.7%, specificity = 91.7%) and RI ≥ 1.08 (AUC = 0.83, sensitivity = 74.3%, specificity = 85.0%) as an optimal cut-off value associated with maxLCBI$_{4mm} \geq 400$ (Fig. 1E and F). Low attenuation plaque volume defined by this cut-off value (CT density <32.9) was significantly correlated to maxLCBI$_{4mm}$ ($r = 0.74$, $p < 0.001$, Supplementary Fig. 3).

The frequency of maxLCBI$_{4mm} \geq 400$ was further compared in association with two CCTA features including CT density <32.9 HU and RI ≥ 1.08. The frequency of maxLCBI$_{4mm} \geq 400$ was only 4.0% at lesions without any of these two CT features. Even if any one CT feature existed, the proportion of maxLCBI$_{4mm} \geq 400$ was still low (=52.6%), whereas lesions with both features exhibited the highest frequency of maxLCBI$_{4mm} \geq 400$ (88.5%, $p < 0.001$ for trend) (Fig. 2). Two representative cases are illustrated in Fig. 3.

4. Discussion

CCTA has been shown as a non-invasive modality to detect lipidic plaque associated with future coronary events. However, its validation study is limited. The present study demonstrated that CT density <32.9, as well as the presence of positive remodeling, was significantly associated with maxLCBI$_{4mm} \geq 400$ on NIRS, but spotty calcification and napkin-ring sign did not. Our findings indicate the relationship of CCTA-derived plaque density and RI with lipid-rich plaque *in vivo*.

The threshold of CT density for lipid-rich plaque has been inconsistent. Motoyama et al. have used CT density <30 HU as a low attenuation plaque according to the comparison of CT density with echogenicity on greyscale IVUS [11]. However, given that evaluation of ultrasonic signal intensity is subjective, this cut-off is not invariably reliable. *Ex vivo* analyses proposed 60 or 75 HU as a cut-off, which corresponds to lipid-rich plaque [9]. Since the *ex vivo* condition is characterized as the absence of cardiac motion and the different settings of CT imaging, this may account for different cut-off of CT density at lipid-rich plaque compared to the aforementioned study. We observed that CT density was associated with NIRS-derived maxLCBI$_{4mm}$, and its best cut-off value for maxLCBI$_{4mm} \geq 400$ was 32.9. Recent validation studies using coronary specimens have demonstrated that the extent of maxLCBI$_{4mm}$ favourably reflects the presence of lipid-rich plaque containing necrotic core. In particular, maxLCBI$_{4mm} \geq 400$ was an independent NIRS-derived feature, which enables to differentiate culprit lesions of ACS containing much lipid content from non-culprit ones [14]. Furthermore, the LRP study elucidated that maxLCBI$_{4mm} \geq 400$ predicted future coronary events [16,23]. These findings support that the current cut-off of CT density could be more reliable compared to greyscale-IVUS-derived one.

Positive remodeling has been reported as another morphological feature of lipid-rich plaques [24–26]. In our analysis, RI was positively correlated to maxLCBI$_{4mm}$. Of note, its cut-off value to predict maxLCBI$_{4mm} \geq 400$ was 1.08. As mentioned above, considering that maxLCBI$_{4mm} \geq 400$ is a histologically validated measure, which predicts future cardiovascular events, our cut-off value may be clinically applicable to detect lipid-rich lesion. Whether this cut-off is better to predict future events requires further investigation.

While CT density and positive remodeling independently associate with maxLCBI$_{4mm} \geq 400$, its accuracy to predict lipid-rich lesion depends on the number of these CCTA features at coronary lesions. In particular, the presence of one feature is not satisfactory to predict maxLCBI$_{4mm} \geq 400$. As shown in Figs. 2 and 52.6% of lesions with one

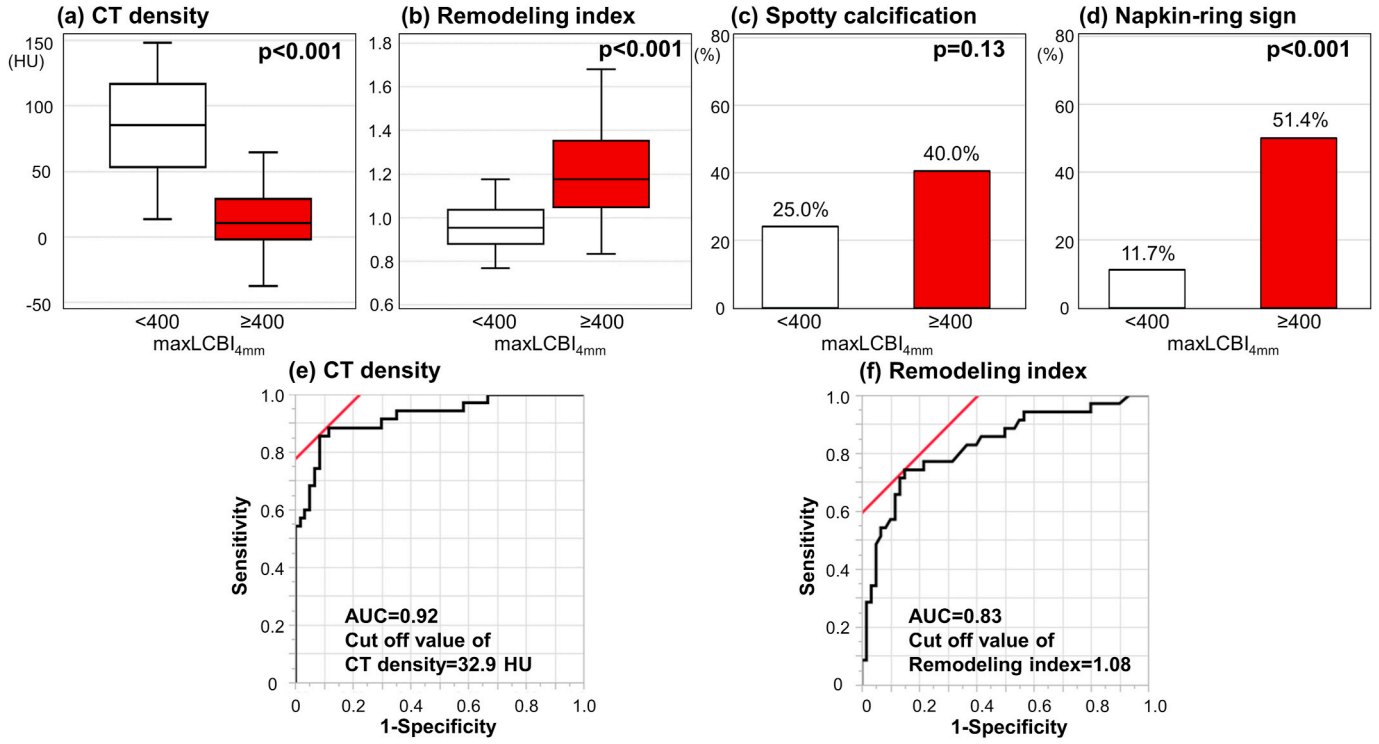

Fig. 1. Comparison of CCTA measures between analyzed coronary lesions with and without maxLCBI$_{4mm} \geq 400$ and ROC curve analysis for predicting maxLCBI$_{4mm} \geq 400$.

(A) CT density. (B) Remodeling index. (C) Spotty calcification. (D) Napkin-ring sign. (E) ROC curve analysis of CT density. (F) ROC curve analysis of remodeling index. CCTA = computed tomography coronary angiography, CT = computed tomography, HU = Hounsfield unit, maxLCBI$_{4mm}$ = maximum 4-mm Lipid Core Burden Index, ROC = receiver operating characteristics.

Table 2
Univariable and multivariable analysis for maxLCBI$_{4mm}$ ≥ 400.

	Univariable analysis					Multivariable analysis				
	OR	95%CI			*p* value	OR	95%CI			*p* value
CT density	0.95	0.92	–	0.97	<0.001	0.95	0.93	–	0.97	<0.001
Positive remodeling	16.25	5.71	–	46.20	<0.001	7.71	1.37	–	43.41	0.02
Spotty calcification	2.00	0.81	–	4.89	0.13					
Napkin-ring sign	8.02	2.86	–	22.45	<0.001	0.45	0.07	–	2.97	0.41

CI = confidence interval, CT = computed tomography, maxLCBI$_{4mm}$ = maximum-4mm lipid core burden index, OR = odds ratio.

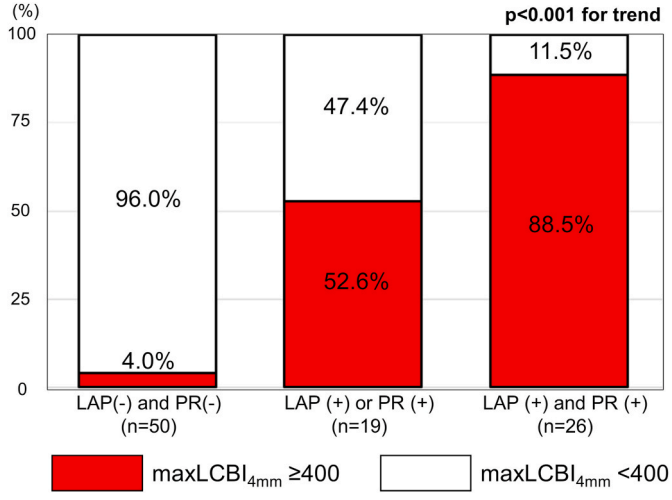

Fig. 2. The frequency of maxLCBI$_{4mm}$ ≥ 400 at analyzed lesions in association with the number of CT-derived morphological features.
CT = computed tomography, LAP = low attenuation plaque (= CT density <32.9), maxLCBI$_{4mm}$ = maximum 4-mm lipid core burden index, PR = positive remodeling (= remodeling index ≥1.08).

feature exhibited maxLCBI$_{4mm}$ ≥ 400 and the remaining 47.4% of those was not necessarily NIRS-derived lipid-rich plaque *in vivo*. Similar findings were reported by another study on intravascular imaging and histological analysis [27]. In this study, combining two IVUS-derived plaque features (plaque burden and RI) has improved c-statistics to predict histological fibroatheroma compared to the presence of only one feature. These findings underscore the concomitance of two CCTA-derived plaque features to better evaluate the presence of lipid-rich plaque.

Spotty calcification and napkin-ring sign were not independent features associated with maxLCBI$_{4mm}$ ≥ 400. Lipid-rich plaque is frequently accompanied by the presence of spotty calcification. However, due to the limited resolution of CCTA imaging for visualizing this speckle calcification pattern [28], it may be difficult to evaluate the relationship of CCTA-derived spotty calcification with maxLCBI$_{4mm}$. With regard to napkin-ring sign, while culprit lesions in patients with acute coronary syndrome more likely presents this feature, the sensitivity of napkin-ring sign to detect fibroatheroma *ex vivo* is only 24.4%, potentially due to its subjectivity [4]. Napkin-ring sign may not be practically useful for detection of lipid-rich lesions. A recent study has reported better accuracy of whole-heart coverage CT scanner to quantify coronary plaque volume [29]. This new technology may further improve the ability of CCTA imaging to characterize plaque quantity and quality.

Several caveats should be noted. Firstly, this study is a single-center retrospective observational study. Secondly, CCTA imaging was used according to each physician's discretion. This may cause a potential bias to select study population. Thirdly, the current study did not specifically set CT acquisition parameters (kV, and mAs) and lumen contrast concentration. However, the correlation between CT density and maxLCBI$_{4mm}$ was consistently observed in all subgroups stratified by the median value of kV, mAs and lumen contrast density, respectively (Supplementary Fig. 4). Lastly, as all patients had CAD requiring PCI with a frequent use of a statin prior to CCTA imaging, it is unknown whether the current findings can be translated to the setting of primary prevention.

In conclusion, CT density <32.9 and positive remodeling were an independent determinant of maxLCBI$_{4mm}$ ≥ 400 measured by NIRS. Coronary lesions with one of these features are less likely to correspond to lipid-rich plaque, whereas its frequency increased at lesions with both features. Our findings highlight the importance of CT density and positive remodeling, especially concomitance of these plaque features to accurately identify a lipid-rich lesion *in vivo*.

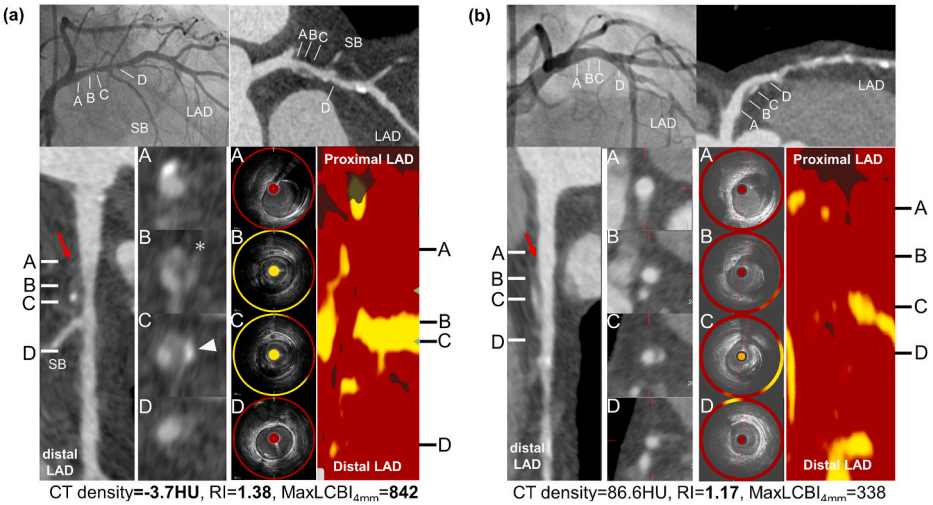

Fig. 3. Representative cases.
(A) A 70 year-old man was hospitalized to receive elective PCI. CCTA prior to PCI visualized an intermediate stenosis at the middle segment of his LAD. In addition to low CT density (CT density = −3.7HU), positive remodeling (RI = 1.38) (red arrow), spotty calcification (arrow head) and napkin-ring sign (asterisk) were observed at this lesion. On NIRS imaging, maxLCBI$_{4mm}$ at the corresponding site was 842.
(B) A 63 year-old man presented silent myocardial ischemia. CCTA imaging showed mild and severe stenoses at the proximal and the middle segment of his LAD, respectively. The mild stenosis exhibited positive remodeling (RI = 1.17) (red arrow), but CT density was 86.6. NIRS imaging showed a low level of maxLCBI$_{4mm}$ (338) at this lesion. CT = computed tomography, HU = Hounsfield units, LAD = left anterior descending artery, maxLCBI$_{4mm}$ = maximum 4-mm Lipid Core Burden Index, SB = septal branch, RI = remodeling index.

CRediT authorship contribution statement

Satoshi Kitahara: Conceptualization, Methodology, Investigation, Data curation, Writing – original draft. **Yu Kataoka:** Conceptualization, Methodology, Investigation, Writing – review & editing, Supervision. **Hiroyuki Miura:** Methodology, Investigation, Writing – review & editing. **Tatsuya Nishii:** Methodology, Writing – review & editing. **Kunihiro Nishimura:** Formal analysis, Writing – review & editing. **Kota Murai:** Writing – review & editing. **Takamasa Iwai:** Writing – review & editing. **Hayato Nakamura:** Writing – review & editing. **Hayato Hosoda:** Writing – review & editing. **Hideo Matama:** Writing – review & editing. **Takahito Doi:** Writing – review & editing. **Takahiro Nakashima:** Writing – review & editing. **Satoshi Honda:** Writing – review & editing. **Masashi Fujino:** Writing – review & editing. **Kazuhiro Nakao:** Writing – review & editing. **Shuichi Yoneda:** Writing – review & editing. **Kensaku Nishihira:** Writing – review & editing. **Tomoaki Kanaya:** Writing – review & editing. **Fumiyuki Otsuka:** Writing – review & editing. **Yasuhide Asaumi:** Writing – review & editing. **Kenichi Tsujita:** Writing – review & editing. **Teruo Noguchi:** Writing – review & editing. **Satoshi Yasuda:** Writing – review & editing, Supervision, Project administration.

Declaration of competing interest

The authors declare the following financial interests/personal relationships which may be considered as potential competing interests: Yu Kataoka has received research support from Nipro and Abbott, and honoraria from Nipro, Abbott, Kowa, Amgen, Sanofi, Astellas, Takeda and Daiichi-Sankyo. The other authors have nothing to disclose.

Acknowledgments

We acknowledge Miss Yoshiko Yoshioka for her support to collect data.

Appendix A. Supplementary data

Supplementary data to this article can be found online at https://doi.org/10.1016/j.atherosclerosis.2021.02.019.

References

[1] E. Falk, Plaque rupture with severe pre-existing stenosis precipitating coronary thrombosis. Characteristics of coronary atherosclerotic plaques underlying fatal occlusive thrombi, Br. Heart J. 50 (2) (1983) 127–134, https://doi.org/10.1136/hrt.50.2.127.

[2] R. Virmani, F.D. Kolodgie, A.P. Burke, A. Farb, S.M. Schwartz, Lessons from sudden coronary death: a comprehensive morphological classification scheme for atherosclerotic lesions, Arterioscler. Thromb. Vasc. Biol. 20 (5) (2000) 1262–1275, https://doi.org/10.1161/01.atv.20.5.1262.

[3] E.S. Kröner, J.E. van Velzen, M.J. Boogers, H.M. Siebelink, M.J. Schalij, et al., Positive remodeling on coronary computed tomography as a marker for plaque vulnerability on virtual histology intravascular ultrasound, Am. J. Cardiol. 107 (12) (2011) 1725–1729, https://doi.org/10.1016/j.amjcard.2011.02.337.

[4] P. Maurovich-Horvat, C.L. Schlett, H. Alkadhi, M. Nakano, F. Otsuka, et al., The napkin-ring sign indicates advanced atherosclerotic lesions in coronary CT angiography, JACC Cardiovasc Imaging 5 (12) (2012) 1243–1252, https://doi.org/10.1016/j.jcmg.2012.03.019.

[5] K. Pohle, S. Achenbach, B. Macneill, D. Ropers, M. Ferencik, et al., Characterization of non-calcified coronary atherosclerotic plaque by multi-detector row CT: comparison to IVUS, Atherosclerosis 190 (1) (2007) 174–180, https://doi.org/10.1016/j.atherosclerosis.2006.01.013.

[6] J.E. van Velzen, F.R. de Graaf, M.A. de Graaf, J.D. Schuijf, L.J. Kroft, et al., Comprehensive assessment of spotty calcifications on computed tomography angiography: comparison to plaque characteristics on intravascular ultrasound with radiofrequency backscatter analysis, J. Nucl. Cardiol. 18 (5) (2011) 893–903, https://doi.org/10.1007/s12350-011-9428-2.

[7] G. Feuchtner, J. Kerber, P. Burghard, W. Dichtl, G. Friedrich, et al., The high-risk criteria low-attenuation plaque <60 HU and the napkin-ring sign are the most powerful predictors of MACE: a long-term follow-up study, Eur Heart J Cardiovasc Imaging 18 (7) (2017) 772–779, https://doi.org/10.1093/ehjci/jew167.

[8] K. Otsuka, S. Fukuda, A. Tanaka, K. Nakanishi, H. Taguchi, et al., Napkin-ring sign on coronary CT angiography for the prediction of acute coronary syndrome, JACC Cardiovasc Imaging 6 (4) (2013) 448–457, https://doi.org/10.1016/j.jcmg.2012.09.016.

[9] D. Han, S. Torii, K. Yahagi, F.Y. Lin, J.H. Lee, et al., Quantitative measurement of lipid rich plaque by coronary computed tomography angiography: a correlation of histology in sudden cardiac death, Atherosclerosis 275 (2018) 426–433, https://doi.org/10.1016/j.atherosclerosis.2018.05.024.

[10] S. Komatsu, A. Hirayama, Y. Omori, Y. Ueda, I. Mizote, et al., Detection of coronary plaque by computed tomography with a novel plaque analysis system, 'Plaque Map', and comparison with intravascular ultrasound and angioscopy, Circ. J. 69 (1) (2005) 72–77, https://doi.org/10.1253/circj.69.72.

[11] S. Motoyama, T. Kondo, H. Anno, A. Sugiura, Y. Ito, et al., Atherosclerotic plaque characterization by 0.5-mm-slice multislice computed tomographic imaging, Circ. J. 71 (3) (2007) 363–366, https://doi.org/10.1253/circj.71.363.

[12] C.L. Schlett, P. Maurovich-Horvat, M. Ferencik, H. Alkadhi, P. Stolzmann, et al., Histogram analysis of lipid-core plaques in coronary computed tomographic angiography: ex vivo validation against histology, Invest. Radiol. 48 (9) (2013) 646–653, https://doi.org/10.1097/RLI.0b013e31828fdf9f.

[13] J. Wang, Y.J. Geng, B. Guo, T. Klima, B.N. Lal, et al., Near-infrared spectroscopic characterization of human advanced atherosclerotic plaques, J. Am. Coll. Cardiol. 39 (8) (2002) 1305–1313, https://doi.org/10.1016/s0735-1097(02)01767-9.

[14] R.D. Madder, R. Puri, J.E. Muller, J. Harnek, M. Götberg, et al., Confirmation of the intracoronary near-infrared spectroscopy threshold of lipid-rich plaques that underlie ST-segment-elevation myocardial infarction, Arterioscler. Thromb. Vasc. Biol. 36 (5) (2016) 1010–1015, https://doi.org/10.1161/ATVBAHA.115.306849.

[15] C.M. Gardner, H. Tan, E.L. Hull, J.B. Lisauskas, S.T. Sum, et al., Detection of lipid core coronary plaques in autopsy specimens with a novel catheter-based near-infrared spectroscopy system, JACC Cardiovasc Imaging 1 (5) (2008) 638–648, https://doi.org/10.1016/j.jcmg.2008.06.001.

[16] S. Waxman, S.R. Dixon, P. L'Allier, J.W. Moses, J.L. Petersen, et al., In vivo validation of a catheter-based near-infrared spectroscopy system for detection of lipid core coronary plaques: initial results of the SPECTACL study, JACC Cardiovasc Imaging 2 (7) (2009) 858–868, https://doi.org/10.1016/j.jcmg.2009.05.001.

[17] S. Abbara, P. Blanke, C.D. Maroules, M. Cheezum, A.D. Choi, et al., SCCT guidelines for the performance and acquisition of coronary computed tomographic angiography: a report of the society of cardiovascular computed tomography guidelines committee: endorsed by the north American society for cardiovascular imaging (NASCI), J Cardiovasc Comput Tomogr 10 (6) (2016) 435–449, https://doi.org/10.1016/j.jcct.2016.10.002.

[18] U. Hoffmann, F. Moselewski, K. Nieman, I.K. Jang, M. Ferencik, et al., Noninvasive assessment of plaque morphology and composition in culprit and stable lesions in acute coronary syndrome and stable lesions in stable angina by multidetector computed tomography, J. Am. Coll. Cardiol. 47 (8) (2006) 1655–1662, https://doi.org/10.1016/j.jacc.2006.01.041.

[19] S. Gauss, S. Achenbach, T. Pflederer, A. Schuhbäck, W.G. Daniel, et al., Assessment of coronary artery remodelling by dual-source CT: a head-to-head comparison with intravascular ultrasound, Heart 97 (12) (2011) 991–997, https://doi.org/10.1136/hrt.2011.223024.

[20] Y. Kataoka, R. Puri, J. Andrews, S. Honda, K. Nishihira, et al., In vivo visualization of lipid coronary atheroma with intravascular near-infrared spectroscopy, Expert Rev. Cardiovasc Ther. 15 (10) (2017) 775–785, https://doi.org/10.1080/14779072.2017.1367287.

[21] R.D. Madder, J.A. Goldstein, S.P. Madden, R. Puri, K. Wolski, et al., Detection by near-infrared spectroscopy of large lipid core plaques at culprit sites in patients with acute ST-segment elevation myocardial infarction, JACC Cardiovasc. Interv. 6 (8) (2013) 838–846, https://doi.org/10.1016/j.jcin.2013.04.012.

[22] M. Marwan, M.A. Taher, K. El Meniawy, H. Awadallah, T. Pflederer, et al., In vivo CT detection of lipid-rich coronary artery atherosclerotic plaques using quantitative histogram analysis: a head to head comparison with IVUS, Atherosclerosis 215 (1) (2011) 110–115, https://doi.org/10.1016/j.atherosclerosis.2010.12.006.

[23] R. Waksman, C. Di Mario, R. Torguson, Z.A. Ali, V. Singh, et al., Identification of patients and plaques vulnerable to future coronary events with near-infrared spectroscopy intravascular ultrasound imaging: a prospective, cohort study, Lancet 394 (10209) (2019) 1629–1637, https://doi.org/10.1016/S0140-6736(19)31794-5.

[24] P. Schoenhagen, K.M. Ziada, S.R. Kapadia, T.D. Crowe, S.E. Nissen, et al., Extent and direction of arterial remodeling in stable versus unstable coronary syndromes : an intravascular ultrasound study, Circulation 101 (6) (2000) 598–603, https://doi.org/10.1161/01.cir.101.6.598.

[25] E. Conte, A. Annoni, G. Pontone, S. Mushtaq, M. Guglielmo, et al., Evaluation of coronary plaque characteristics with coronary computed tomography angiography in patients with non-obstructive coronary artery disease: a long-term follow-up

study, Eur Heart J Cardiovasc Imaging 18 (10) (2017) 1170–1178, https://doi.org/10.1093/ehjci/jew200.

[26] H.J. Chang, F.Y. Lin, S.E. Lee, D. Andreini, J. Bax, et al., Coronary atherosclerotic precursors of acute coronary syndromes, J. Am. Coll. Cardiol. 71 (22) (2018) 2511–2522, https://doi.org/10.1016/j.jacc.2018.02.079.

[27] R. Puri, R.D. Madder, S.P. Madden, S.T. Sum, K. Wolski, et al., Near-infrared spectroscopy enhances intravascular ultrasound assessment of vulnerable coronary plaque: a combined pathological and in vivo study, Arterioscler. Thromb. Vasc. Biol. 35 (11) (2015) 2423–2431, https://doi.org/10.1161/ATVBAHA.115.306118.

[28] A.P. Burke, D.K. Weber, F.D. Kolodgie, A. Farb, A. Taylor, et al., Pathophysiology of calcium deposition in coronary arteries, Herz 26 (4) (2001) 239–244, https://doi.org/10.1007/pl00002026.

[29] E. Conte, S. Mushtaq, G. Pontone, L. Li Piani, P. Ravagnani, et al., Plaque quantification by coronary computed tomography angiography using intravascular ultrasound as a reference standard: a comparison between standard and last generation computed tomography scanners, Eur Heart J Cardiovasc Imaging 21 (2) (2020) 191–201, https://doi.org/10.1093/ehjci/jez089.